ITC 3/53
Information Technology and Control
Vol. 53 / No. 3/ 2024
pp. 710-723
DOI 10.5755/j01.itc.53.3.35741

Design Path of Robot Motion Control System Based on Graphic Element Information

Received 2023/11/27 | Accepted after revision 2024/03/25

HOW TO CITE: Huang, Z., Liang, B. (2024). Design Path of Robot Motion Control System Based on Graphic Element Information. *Information Technology and Control*, 53(3), 710-723. https://doi.org/10.5755/j01.itc.53.3.35741

Design Path of Robot Motion Control System Based on Graphic Element Information

Zhongshi Huang
Department of Mechanical Engineering, Baise Vocational College, Baise, 533000, China

Binbin Liang
Department of Economic Management, Baise Vocational College, Baise, 533000, China

Corresponding author: hzs20192023520@126.com

As the core of the numerical control system, the motion control system of robots determines the machining efficiency and quality of the numerical control machine tool. This study aims to improve the stability of robot motion control systems, thereby further enhancing the efficiency and economic benefits of numerical control machine tools. Therefore, the robot motion control system based on the graphic element information and machining path is designed. Combined with simulated annealing algorithm and S-type acceleration and deceleration control algorithm, the robot motion control system is more accurate and efficient. From the findings, compared with the traditional motion control system, the improved system significantly reduced the empty stroke length by more than 50%. The S-type acceleration and deceleration control algorithm effectively improved the stability of the swing arm and reduced the contour error. On the premise of ensuring the cutting accuracy, the improved method could improve the smoothness of the part, reduce burrs, and make the part more suitable. The proposed method can effectively improve the performance of robot motion control system and meet the requirements for product quality in practical applications.

KEYWORDS: Graphic Element Information; Machining path; Automation; Control system; S-type acceleration and deceleration control algorithm.

1. Introduction

With the rapid development of China's manufacturing industry, robot motion system has shown obvious advantages compared with manual in controlling quality, work efficiency, some high-risk links, and cost [5, 14]. The application of robots in industrial manufacturing can significantly improve production efficiency and product quality while significantly reducing workload and work costs. As an important tool for the development of modern industrial engineering, industrial robots have been widely used in various industries [13]. How to improve the motion control system of robots is also the research direction [7, 24]. This study aims to improve the accuracy and efficiency of the robot motion control system by combining Simulated Annealing (SA) algorithm with S-type acceleration and deceleration control algorithm. SA algorithm, as a heuristic optimization algorithm, can effectively avoid the local optimal and find the global optimal solution. Meanwhile, the S-type acceleration and deceleration control algorithm can generate a smooth acceleration curve, which can quickly and accurately control the robot's motion. The combination of the two methods effectively improves the performance of the robot motion control system in speed planning and trajectory optimization. Shao et al. [15] designed an improved robot that combined industrial computer and STM32 to improve the motion accuracy and relative positioning ability of the overhead wire inspection robot. The empirical results showed that it had high motion and positioning accuracy, which met the work requirements of the inspection robot. Li [6] developed a 6-DOF industrial robot recognition method to achieve accurate motion control and accurate payload estimation of industrial robots. Comparative experiments showed that the proposed controller could estimate the payload as the true value and exhibit better tracking performance. At present, robot motion systems still have room for improvement in terms of improving stability and reducing economic losses. Therefore, it is important to improve the design of robot motion control system to ensure stability, accuracy and practical engineering application.

The innovative of the research is as follows. For the design of robot motion paths, the S-type acceleration and deceleration method has been innovatively introduced to improve the stability of the robot motion control system, hoping to improve the performance of the Numerical Control (NC) robot motion control system.

The contributions of the research are as follows. The annealing algorithm is applied to design robot machining paths to optimize the motion path. Then, the study adopts the S-shaped curve acceleration and deceleration method to maintain the stability of the robot motion control module. The sudden speed changes caused by excessive acceleration is solved, avoiding robot vibration and improving the performance of the NC robot motion control system. The obtained robot motion path is superior to traditional methods.

2. Related Work

In recent years, research on intelligent robots has received extensive attention. To improve the effectiveness and accuracy of robots in work tasks, many scholars have optimized it. Liu et al. [10] proposed a robot motion controller based on automatic parameter adjustment to improve the anti-interference performance of the robot in practical applications. The state equation and particle swarm optimization algorithm were combined to design the robot motion controller. The results showed that the method achieved the expected time and stability performance. Bao et al. [1] proposed a new decoupling motion control algorithm based on robot attitude calculation. Four fuzzy proportional calculus controllers were used to independently control the robot motion in all directions. The results showed that this method improved the flexibility and accuracy of robot motion. Zhao et al. [23] proposed a feedback controller method to complete periodic motion tasks. The adaptive characteristics of the central mode generator were enhanced to reduce the resistance in the system. The results showed that this method could effectively simulate and identify human body system. To solve the time problem of traditional robot pivot motion, Lin [8] proposed an artificial intelligence control algorithm based on steering motion. The results showed that the steering speed of the proposed wheeled soccer robot was 30% higher than that of the traditional robot, which effectively solved the

steering delay. Lin et al. [9] proposed a vision-based controller method to improve the pickup and placement functions of cable-suspended robots. The test showed that this method was applicable to cranes, and other large-scale manufacturing equipment requiring cable-driven robots.

S-AAD is a commonly used method in motion control systems to address sudden acceleration changes. By introducing the linear acceleration variable, the speed calculation curve shows an S-shape. The sudden acceleration changes in the traditional S-AAD cause machine tool vibration and affect the surface quality of the components. In response to this problem, Luo et al. [12] reduced the slope change by determining the speed-sensitive point of the curve to reduce the flexible impact. The results showed that this method effectively reduced flexible impact and improved machining accuracy. Wang et al. [19] combined the S-AAD with B-spline curve interpolation algorithm to realize the smooth speed transition. The simulation results showed that the algorithm realized the smooth acceleration transition in NC machining. Jia et al. [4] proposed a smooth S-AAD based on jounce finite contour to solve the insufficient smoothness of existing tool paths. The results showed that the method had good performance in motion smoothness and surface quality. Yu et al. proposed a four-order S-AAD to solve the step problem in the acceleration phase of traditional S-AAD in the NC machining. In addition, the uniform speed compensation algorithm was used to solve the time consumption and instability under different accuracy requirements. The results showed that the method improved the motion stability of NC machining while meeting real-time requirements [21]. To control the real-time speed of the robot during movement, Xu et al. [20] adopted the S-AAD to control the physical axis of the robot. The results showed that this method could reduce the trajectory error of the robot's physical axis movement process to less than 10^{-4}, with simple operation and smooth speed transition.

To summarize, robot automatic control systems and S-AAD have been widely applied in their respective fields. However, there is relatively insufficient research on optimizing the design of robot control systems by combining the two. Therefore, when designing the motion control system of NC robots, the S-AAD is innovatively introduced based on the primitive information and machining path to improve the stability of the robot motion control system, improving the performance of the NC robot motion control system.

3. Design of Motion Control Model for NC Robot

3.1. Design of Motion Control Model Based on Machining Path

The control content of the motion control system for NC machining robot mainly includes two parts. The first is that the NC robot arrives at the designated place according to the command. The second is that robots complete processing, cutting, welding and other tasks. During the control process, the robot motion system is completed with the graphic element information and machining path [11]. In all NC equipment, the interpolation algorithm is embedded in the motion control module to ensure processing accuracy and production process stability. The motion control model of NC robot needs to read and process the primitive data before reading the data. In the drawing, the data to be processed twice includes arc interpolation and poly-line. Arc interpolation requires arc start point, end point and radius. The secondary processing formula is shown in Formula (1).

$$\begin{cases} x = O.x + r \times \sin(\partial) \\ y = O.y + r \times \cos(\theta) \end{cases}. \quad (1)$$

In Formula (1), the coordinate of the arc center is $(O.x, O.y)$. ∂ is the starting angle. θ is the ending angle. A poly-line is a curve formed by splicing straight lines and arcs. In DXF, a poly-line stores the endpoint of each segment. The fixed points $(ps.x, ps.y)$ and $(pe.x, pe.y)$ are the convexity *bul* corresponding to the line segment. When the convexity is 0, the line segment is straight. When the convexity is greater than 0, the intermediate variable is m. The calculation is shown in Formula (2).

$$m = \left(1/bul - bul\right)/2 \quad (1)$$

The relationship can be obtained from Formula (3).

$$\begin{cases} O.x = (ps.x + pe.x - (pe.y - ps.y) \times m)/2 \\ O.y = (ps.y + pe.y - (pe.x - ps.x) \times m)/2 \end{cases}. \quad (3)$$

In Formula (3), $O.x$ is the horizontal coordinate of the arc center. $O.y$ is the ordinate of the circular arc center. The fixed points $(ps.x, ps.y)$ and $(pe.x, pe.y)$ are the convexity bul corresponding to the line segment. m is the intermediate variable. The designer cannot draw the drawing according to the optimal path during the drawing process. Computer-aided design records the data according to the drawing order of the entity, instead of automatically calculating the optimal path, resulting in many empty strokes and meaningless cuts when processing parts. This greatly slows down production efficiency and causes excessive wear. Therefore, the machining path is improved based on the SA. SA is a greedy algorithm. Compared with the traditional greedy algorithm, SA can jump out of the local optimal and make the result close to the global optimal solution by introducing specific criteria, which is one of the early algorithms introduced to solve the optimization problem. SA starts from a higher initial temperature according to the metal processing and annealing [3, 22]. As the number of iterations increases, the annealing simulation temperature decreases continuously to find the global optimal solution. During the annealing process, the relationship between the energy state of particles and temperature conforms to the Boltzmann distribution. The distribution function is shown in Formula (4).

$$P = \begin{Bmatrix} 1 df < 0 \\ e^{-\frac{df}{KT}}, df \geq 0 \end{Bmatrix}. \quad (4)$$

In Formula (4), $df = E(X_j) - E(X_i)$, and i is the current moment. j refers to the next moment. K is the Boltzmann constant. e is the natural index. T is the temperature. In the SA algorithm, Metropolis method is introduced to simulate the metal solid from constant temperature to thermal equilibrium. $df < 0$ represents the cooling process. In the actual annealing process, df should always be less than 0. Therefore, $df / KT < 0$. The value range of $P(df)$ is (0,1). With the decrease of temperature T, $P(df)$ decreases gradually. The SA function is shown in Figure 1 [2, 17].

Figure 1 shows the commonalities abstracted from the simulation and combinatorial optimization problems of solid material cooling processes in reality. To find the minimum value of the function, the initial function value is set to $F(x_0)$. When the program

Figure 1
Optimization Process of Simulated Annealing Algorithm

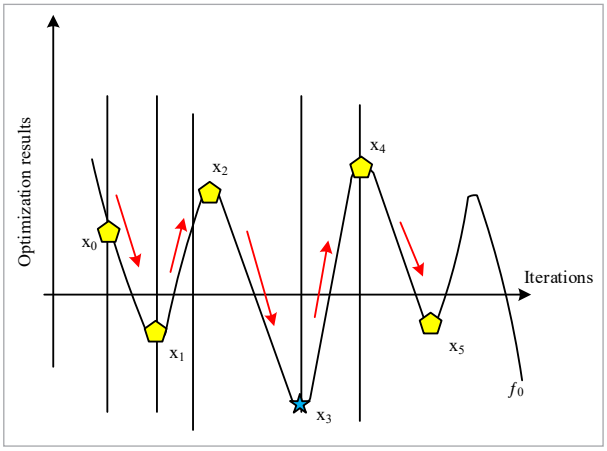

starts to iterate, the initial value of the control parameters, the decay factor, the number of iterations and the stop condition produce a new solution. It is considered that the new solution is better than the previous one, and finally avoids the local optimal trap to get the global optimal $f(x_m)$. In the calculation process, to improve the calculation speed and reduce the computational complexity, the current objective function should be determined by the elements obtained by exchanging the current solution with the new solution. The calculation process of SA is shown in Figure 2. In Figure 2, firstly, a new solution is generated based on the initial objective function, thereby obtaining a new objective function. Then, the difference between the two objective functions is determined. When the difference meets the preset conditions, the new solution is accepted. Otherwise, the new solution is recalculated. Then, the number of iterations of the algorithm is determined. If the iteration satisfies the optimal solution, the optimal result is obtained. Otherwise, the annealing temperature is lowered and the iteration is repeated until the optimal solution is obtained.

$$P(x_1 \Rightarrow x_2) = \begin{cases} 1 & f(x_2) \leq f(x_1) \\ \exp\left(\dfrac{f(x_1) - f(x_2)}{t}\right) & f(x_2) > f(x_1) \end{cases}. \quad (5)$$

In the SA algorithm, there are generally two ways to deal with the problem, the outer loop and the inner loop. The transfer probability corresponding to Metropolis criterion in the inner loop is shown in Formula (5).

Figure 2
Flow Chart of Simulated Annealing Algorithm

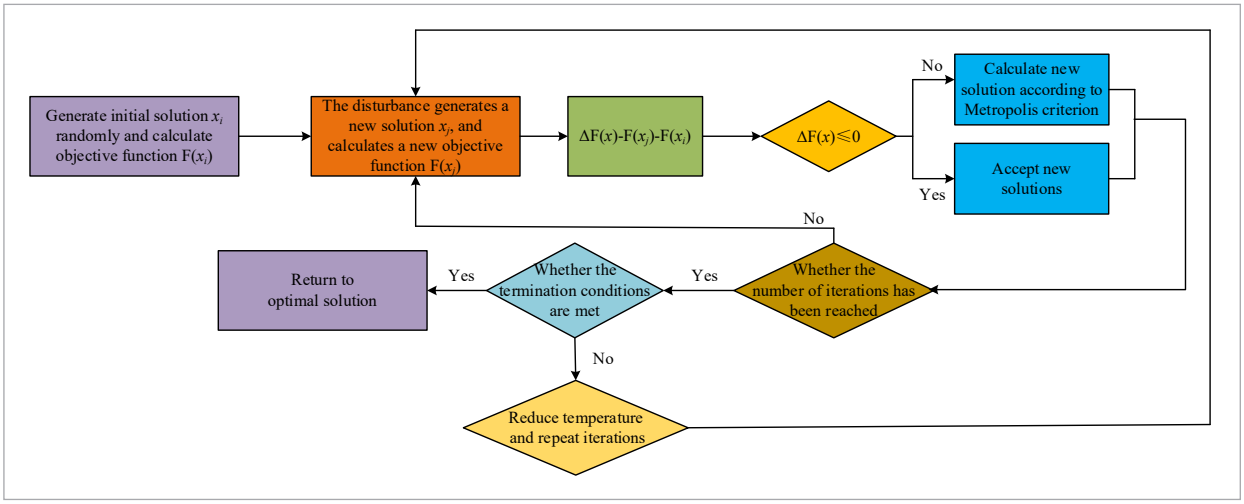

In Formula (5), t is the control parameter. x_1 and x_2 are two new solutions of the previous iteration and this iteration. After completing a cycle, the temperature condition is judged. If the temperature does not reach the set value, the cycle is continued. If the temperature meets the established conditions, the optimization is completed and the optimization results are output.

3.2. Stability Design of Motion Control Module

To maintain the stability and accuracy of machining complex parts, the interpolation algorithm module is embedded in the NC system to process the machining path density. To shorten the acceleration and deceleration time, ensure the stability of robot movement and reduce system impact, the acceleration and deceleration of equipment needs to be controlled. Acceleration and deceleration control is the basis of stability in NC system. In the machining path optimized by SA, the S-AAD is used to maintain the stability of the motion control module. The S-AAD control is based on the linear acceleration and deceleration control method to restrict the Jerk, thereby eliminating sudden changes in acceleration and improving algorithm smoothness [16, 18]. The control process is divided into seven different motion stages. After introducing the concept of acceleration, the acceleration curve can be continuously changed to avoid the sudden change caused by excessive acceleration, which can avoid robot vibration and improve product processing quality. The S-AAD diagram is shown in Figure 2.

Figure 3
S-Shaped Curve Acceleration and Deceleration Diagram

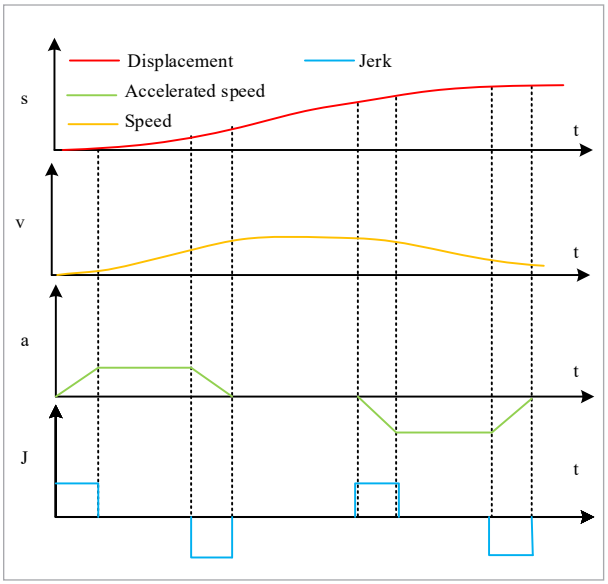

Assuming that the acceleration time is the same in different motion time period, seven different phase relations can be obtained. The acceleration phase relationship is shown in Formula (6).

$$\begin{cases} t_1 = t_3 = t_5 = t_7 = t_j \\ t_2 = t_6 = t_a \\ t_4 = t_v \end{cases}. \quad (6)$$

In Formula (6), t_j is the Jerk. t_a is the acceleration time. t_v is the speed time. The relationship formula for the uniform acceleration stage is shown in Formula (7).

$$\begin{cases} a(t_1) = j_{\max} t_j \\ v(t_1) = \frac{1}{2} j_{\max} t_j^2 \\ s(t_1) = \frac{1}{6} j_{\max} t_j^3 \end{cases} . \quad (7)$$

In Formula (7), a is the acceleration. v is the speed. s is the displacement. The relationship between acceleration and deceleration stages is shown in Formula (8).

$$\begin{cases} a(t_3) = a(t_2) - j_{\max} t_j \\ v(t_3) = j_{\max} t_j^2 + j_{\max} t_j t_a \\ s(t_3) = s(t_2) + v(t_2) t_j + \frac{1}{2} a(t_2) t_j^2 \end{cases} . \quad (8)$$

The relationship formula for uniform velocity stage is shown in Formula (9).

$$\begin{cases} a(t_5) = -j_{\max} t_j \\ v(t_5) = \frac{1}{2} j_{\max} t_j^2 + \frac{1}{2} j_{\max} t_j t_a \\ s(t_5) = s(t_4) + v(t_4) t_j + \frac{1}{2} a(t_4) t_j^2 - \frac{1}{6} j_{\max} t_j^3 \end{cases} . \quad (9)$$

The relationship between deceleration and acceleration stages is shown in Formula (10).

$$\begin{cases} a(t_5) = -j_{\max} t_j \\ v(t_5) = \frac{1}{2} j_{\max} t_j^2 + \frac{1}{2} j_{\max} t_j t_a \\ s(t_5) = s(t_4) + v(t_4) t_j + \frac{1}{2} a(t_4) t_j^2 - \frac{1}{6} j_{\max} t_j^3 \end{cases} . \quad (10)$$

The uniform deceleration stage is shown in Formula (11).

$$\begin{cases} a(t_6) = -j_{\max} t_j \\ v(t_6) - \frac{1}{2} j_{\max} t_j^2 \\ s(t_6) = s(t_5) + a(t_5) t_a + \frac{1}{2} a(t_5) t_a^2 \end{cases} . \quad (11)$$

The deceleration phase is shown in Formula (12).

$$\begin{cases} v(t_7) = 0 \\ a(t_7) = 0 \\ s(t_7) = s(t_6) + v(t_6) t_j + \frac{1}{2} a(t_6) t_j^2 + \frac{1}{6} j_{\max} t_j^2 \end{cases} . \quad (12)$$

In the above formula, the maximum speed, maximum acceleration and maximum Jerk are calculated as known conditions respectively. At the same time, if the speed, acceleration and Jerk are restricted, the planning process of S-AAD control method can be calculated. In the practical application of S-shaped curve, the whole motion trajectory is a collection of multiple path points. After moving from the initial coordinate point to the target coordinate point, the motion process will continue to be repeated. In this movement process, each path needs to be accelerated and decelerated. This will cause frequent start and stop operations of the robot motion system, affecting the motion efficiency and reducing the accuracy of the robot work. Therefore, in order to reduce the impact of the starting and stopping speed at the front and rear ends of the path on the motion system, the speed at the connecting ends is adjusted. On the basis of not changing the original machining path, the research adopts linear transition prospective processing to control the speed at each connecting end point. When dealing with the speed of the connecting end points, the speed of each connecting end point shall not be reduced to zero. The transition speed calculated under the constraint conditions is used as the connection speed between the current phase and the next phase. That is, the current stop speed is used as the initial speed of the next stage, so as to achieve a reasonable transition between the two movements. When determining the forward-looking point, the points with high curvature and sharp corners in the motion trajectory are processed with speed forward-looking. Curvature represents the degree of curvature between two segments of the path. In the calculation process, the curvature values near the four points are calculated by determining any four coordinate point functions, as shown in Figure 4.

In Figure 4, P_1, P_2, P_3, and P_4 represent any four coordinate points. V_1 represents the speed from P_1 to P_2. V_2 represents the speed from P_2 to P_4. R_1 represents the curvature between P_1 and P_2. R_2 represents the curvature between P_2 and P_3. θ represents the angle

Figure 4
Speed Forward Motion Trajectory

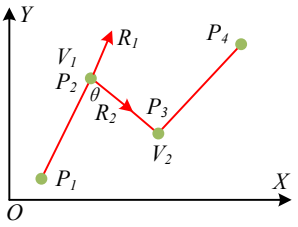

formed between P_1 and P_3. The speed at the end point transition includes the inlet speed and outlet speed at the current stage. The outlet speed at the current stage meets the conditions, as shown in Formula (13).

$$v_{out}^2 \le v_{in}^2 + 2a_i L_i. \tag{13}$$

In Formula (13), v_{in} represents the initial speed of each stage. a_i represents the acceleration of the current phase. L_i represents the displacement of the current phase. v_{out} represents the stopping speed of each stage. The outlet speed of the current stage can be calculated by combining the maximum sudden change speed of the inflection point and the maximum speed of the motion control system, as shown in Formula (14).

$$v_{out} = \min(V_m, V_{out}, V_{\max}). \tag{14}$$

In Formula (14), V_m represents the maximum mutation speed of the inflection point. $V_{\max}$ represents the maximum speed of the motion control system. The starting speed of the next stage is $v_{in} = v_{out}$. Each forward processing speed at the inflection point can be obtained by solving Formula (14) until the last stage. Similarly, each backward processing speed at the inflection point can be calculated. The initial speed and stop speed of each stage can be obtained by combining the speed obtained in the pre-treatment process and the post-treatment process, as shown in Formula (15).

$$\begin{cases} v_{in} = \min(v_{in}, v_{in}^{'}) \\ v_{out} = \min(v_{out}, v_{out}^{'}) \end{cases}. \tag{15}$$

The data obtained after forward-looking processing at each stage is used as the constraint parameter of speed planning in S-AAD for acceleration and deceleration planning.

3.3. Challenges and Limitations in Implementation

A series of challenges and limitations have been encountered when approaching the design path of robotic motion control systems, which provide enlightening results for the research, as well as a glimpse into the limitations of current methods in practical applications. First of all, there are problems with different hardware. Because each robot has its own unique hardware structure, it is very difficult to design and implement a universal motion control system. For example, differences in factors such as drivetrain, encoder resolution, motor torque, etc. between robots may have an impact on motion control performance. To solve this problem, a design method based on graphic element information and processing path is adopted to reduce the dependence on specific hardware details as much as possible.

Secondly, the experimental environment also caused some problems. In the field application process, the diversity of robot operating environment may have impacts on the design of motion control system. For example, factors such as temperature, humidity, noise, and even geographic location can have impacts on system performance. Therefore, the system design is as rigid as possible. Some adjustment mechanisms are designed to adapt to different working environments.

In addition, system performance limitations are another challenge encountered during the implementation process. Due to the limitation of computing resources and processing power, it is a great challenge to design a motion control system that can not only respond in real time but also control accurately. The designed approach requires some compromises, such as finding a balance between real-time and precision.

4. Simulation Analysis and Engineering Application of Robot Motion Control System

4.1. Path Optimization Analysis of Robot Motion Control System

To ensure the accuracy and reliability of the experimental results, the experimental conditions is designed and planned in detail. MATLAB is used to

establish a simulation test environment. Matlab is currently the most widely used simulation development platform, which can utilize multiple tool modules to achieve more detailed visualization analysis for robot motion trajectories. Firstly, a representative type of workpiece is selected, including different shapes and different materials (such as metal or plastic). Secondly, in terms of processing path and speed, the specific processing path and speed are specified in accordance with the predetermined experimental design to gain a deeper understanding of the performance of the motion control system under various working conditions. For example, different types of machining paths (linear and curved) are used to match different machining speeds for testing in multiple scenarios. Considering that environmental factors may affect the experiment results, it is ensured that the experiment is set up to simulate the actual operating conditions, such as the corresponding temperature, humidity, and possible electromagnetic interference in the surrounding environment. At the same time, the accuracy and performance of all measuring tools and processing equipment meet the experimental requirements. Finally, an efficient data acquisition and processing system is used to capture key parameters during the experiment, such as robot joint angle, speed, acceleration, etc. Data processing removes possible outliers and errors to obtain more accurate, sensitive and reliable experimental results. Table 1 shows the drawing optimization effects with different number of machining elements.

From Table 1, when graphic elements increased, the empty stroke of the traditional machining path also increased. When the number of graphic elements was 30, the empty stroke length was 2468.3mm. When the number of graphic elements was 60, the length of empty stroke was 7 times that of 30 elements. After optimization based on SA, when the number of graphic elements was 30, the empty stroke length was 1592.9mm, which was 35.4% less than the traditional machining path. The running time was 0.29s. When the number of graphic elements was 100, the machining path optimized by SA was reduced by 88%, and the running time was 0.79s. When the graphic elements increased, the optimization rate of the optimized path was higher than that of the traditional machining path. When the number of graphic elements exceeded 100, the empty stroke length was reduced by more than 80%, but the running time was longer. Compared with a small number of graphic elements, the running time increased by 0.56s. The drawings of a machined parts are tested. The comparison diagram of path optimization is shown in Figure 5.

The line segment with an arrow in Figure 5 represents the robot motion path. In Figure 5(a), there were 11

Table 1

Comparison of Empty Stroke Length Optimization Results under Different Number of Entities

Number of graphic elements	Before optimization	After optimization	Run time
20	1983.6 mm	1586.88 mm	0.23s
30	2468.3 mm	1592.9 mm	0.29s
60	17248.3 mm	7274.4 mm	0.6s
100	35242.4 mm	4295.3 mm	0.79s
120	42635.9 mm	3410.9 mm	0.84s

Figure 5

Effect of Path Optimization

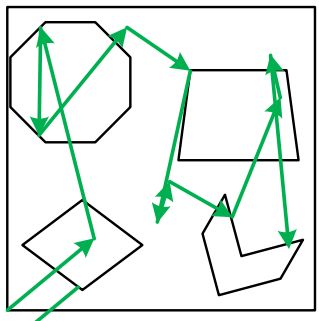

(a) Traditional wayfinding path

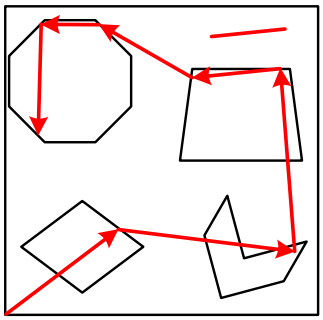

(b) Optimized path

turns in the traditional planning path. There were multiple unnecessary empty trips. In Figure 5(b), the path had 7 turns. Compared to traditional paths, the improved machine motion path reduced unnecessary empty trips by 4 turns. This indicates that the SA algorithm proposed in the study can effectively reduce the empty trips in the machining process and optimize the running trajectory of the robot. In addition, the accuracy change of the system is compared by analyzing the accuracy of the swing arm and the moving path of the NC robot. The control error of swing arm movement when machining two parts with different shapes shows in Figure 6.

Figure 6 shows the cutting accuracy comparison of two different parts. In Figure 6(a), the proposed method could correctly identify the machining path. The error was about 0.3mm, which was within the acceptable range. In Figure 6(b), the error of cutting parts occurred at the corner part of parts, which could be almost ignored. There was no cutting error in the straight section. In Figure 6(c), the machining path error of the comparison algorithm was obvious. There were significant errors in some features. In Figure 6(d), the machining path bend was out of the drawing, and the error exceeded 1mm. In general, the cutting accuracy of the improved NC robot reached more than 99%. It not only meets the production needs, but also has a higher qualification rate than traditional NC machines. The accuracy of the part corners and arcs is higher. The robot motion control system with path processing optimization meets the requirements of movement error and task success rate, which has good control effect.

Figure 6
Drawing and System Cutting Error Diagram

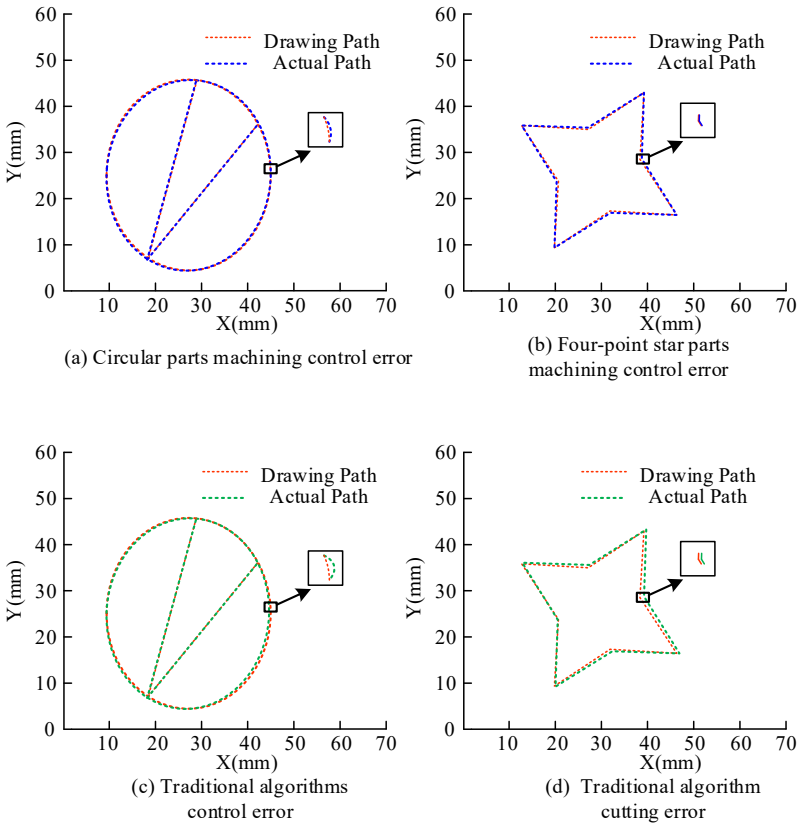

(a) Circular parts machining control error

(b) Four-point star parts machining control error

(c) Traditional algorithms control error

(d) Traditional algorithm cutting error

4.2. Smoothness Analysis of Robot Motion Control System

The initial speed parameters of the S-shaped curve are verified to obtain the best operating speed. The study sets two conditions to verify the S-shaped curve. The first starting speed is 0 mm/s, the maximum running speed is 60 mm/s, the ending speed is 10 mm/s, the maximum acceleration is 30 mm/s^2, and the running distance is 60 mm/s. The second is that the starting speed is 0 mm/s, the maximum running speed is 60 mm/s, the ending speed is 10 mm/s, the maximum acceleration is 30 mm/s^2, and the running distance is 60 mm/s. The speed and acceleration curve of S-AAD under different conditions are shown in Figure 7.

Figure 7

Change of Speed and Acceleration Curve under Different Conditions

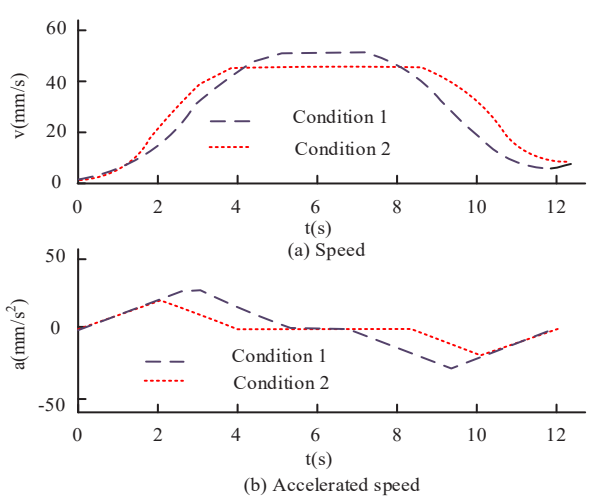

In Figure 7(a), the S-shaped curve had uniform acceleration and deceleration stages in both conditions. The main difference was that the time of maintaining constant speed was inconsistent. From Figure 7(b), in the first condition setting, the S-AAD had a constant speed operation stage. However, limited by the maximum operating speed, there was no uniform acceleration and deceleration stage in the curve. The acceleration and deceleration motion of the curve under the second condition setting had a uniform motion stage. After comprehensive comparison, the parameters under the second condition are taken as the test parameters of S-AAD.

In the NC system, the vibration and impact of the machine tool affect the fluctuation of the swing arm and the smoothness of the machined parts. The smoothness of the part edge cannot meet the standard requirements. This leads to part scrapping, increase the wear rate of the swing arm, and cause additional economic losses. The speed comparison between the traditional algorithm and the research algorithm is shown in Figure 8.

Figure 8

Comparison of Two Algorithms

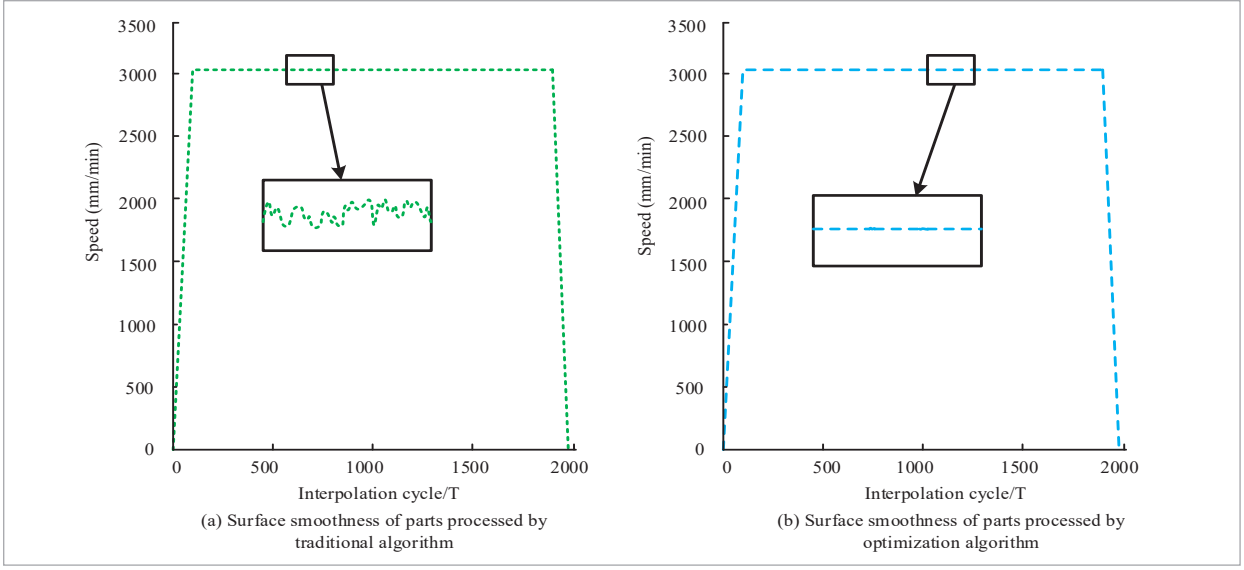

In Figure 8, the speed curves of the two algorithms were roughly the same. The maximum speed of the proposed algorithm was faster than that of the traditional algorithm. In Figure 8(a), the traditional algorithm took 6s to process parts, with frequent fluctuations. In every 200 interpolation cycles, the number of fluctuations reached 30. The part edges were depressed and had low smoothness. In Figure 8(b), it took 5.86s to process parts. Compared with the traditional algorithm, the fluctuation of the research algorithm was not obvious. In every 200 interpolation cycles, the fluctuation period only occurred once, with small fluctuation amplitude. To summarize, the research algorithm had good anti-swing and anti-fluctuation performance compared with the traditional algorithm. According to the automatic control theory, there must be some following error in the control system during processing, which is called contour error. The contour error between traditional algorithm and research algorithm is shown in Figure 9.

Figure 9 shows the contour error between traditional algorithms and the research algorithm. In Figure 9(a), when using traditional algorithms for machining, the contour accuracy fluctuated within a range, resulting in a large number of errors. The error value fluctuated greatly on the transition line segment. When the interpolation period was 400, the contour error varied within [0.5, 3.5]. Figure 9(b) shows the research algorithm for machining contour errors. The error generated by the research algorithm in each interpolation cycle was relatively small, which basically formed a curve. The error value was basically on the fitted curve. The error fluctuation value was significantly reduced. This method maximizes the accuracy of the cutting graph. In 1600 interpolation cycles, the error trends obtained by the two methods were consistent, but the actual errors differed significantly. Therefore, the optimization algorithm can achieve very accurate machining accuracy under the high-precision and high-speed machining. The comparison of part edge processing effect is shown in Figure 10.

Figure 10

Comparison of Part Burr under Two Algorithms

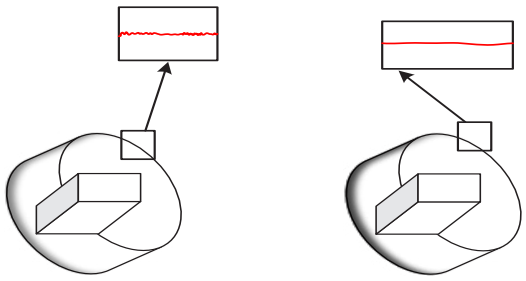

(a) Traditional algorithm part burr

(b) Improved algorithm part burr

Figure 9

Comparison of Contour Error of Two Algorithms

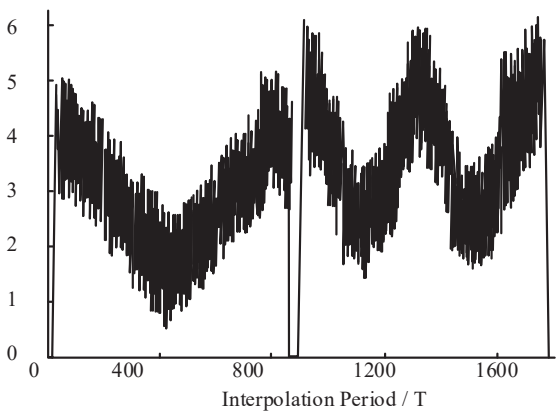

(a) Traditional algorithm contour error

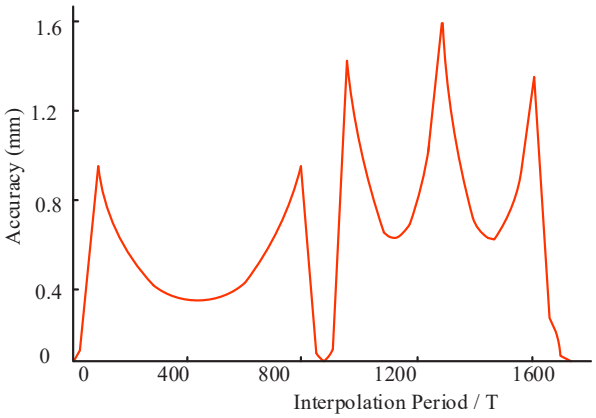

(b) Research algorithm contour error

Table 2
Comparison of Parts Processing under Two Algorithms

Processing method	Traditional algorithm	Improved algorithm
Burr	34	9
Section finish	0.33	1.32
Section roughness	0.376	1.57
Part status	Coarse	Smooth
Depression	29	8

Figure 10(a) shows the parts processed by traditional algorithms. There were many burrs on the edge and the smoothness was low. After improving algorithm, the burr on the edge of the machined part was greatly reduced and the edge was smoother. The parameter comparison of the two algorithms for this part is shown in Table 2.

From Table 2, the number of burrs in the traditional algorithm was 34, and the optimization algorithm was only 9. the optimized algorithm reduced the burr of parts by 25 points compared with the traditional algorithm. The depression reduced by 21 points. The section maintained a high smoothness, and the part state was highly matched with the drawing. Compared with the traditional processing process, the part completion degree was higher. It can better meet the drawing planning and daily production requirements.

Figure 11
Response Curve Contrast

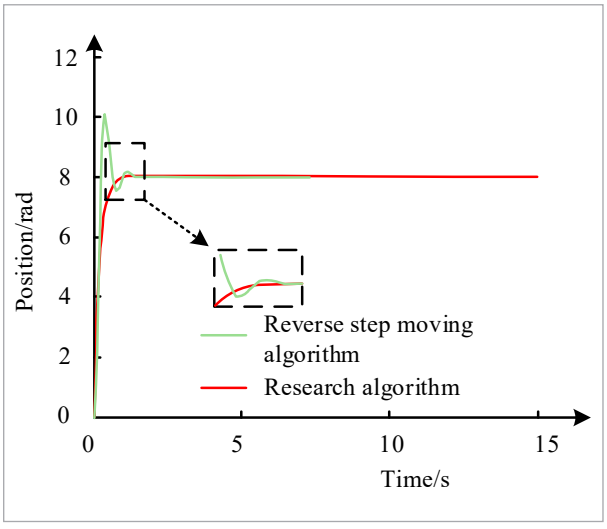

Figure 11 shows the response time comparison between the reverse step algorithm and the research algorithm. It can be seen that the control of the research algorithm effectively inhibits the overshoot, speeds up the response time, which has a better tracking ability to the system input.

5. Conclusion

In conclusion, in robot motion control systems, the integration of digital control technology and graphic element information has greatly improved efficiency and accuracy. The SA reduced unproductive movement, saving up to 88% of time, with a maximum processing time of 0.79s. Furthermore, the S-AAD improved accuracy, ensuring the cutting accuracy of over 99%. Compared with traditional NC machines, it boasts a higher qualification rate, superior cutting precision, and fewer time requirements for executing complex tasks. While the machining is processed at a constant speed, there are minimal fluctuations, contributing to its resistance to oscillatory movement and waveform disturbances. Regardless of the success of this system in this study, there is still room for optimization.

Firstly, there are differences in the structural design of each robot. The factors such as the transmission system and coding resolution of the robot system have impacts on the path control results. In future research, the impact of different transmission systems and coding resolutions in robot systems on path control results will be further analyzed in depth. The optimal transmission system and resolution conditions will be determined. Secondly, during the experiment, the external environment, including temperature, humidity, noise, etc., can also affect the

control results of the robot motion path. The study does not uniformly design the external environment, which may have a certain impact on the results. In future research, the external environment can be uniformly designed to optimize the experimental condition.

References

1. Bao, P., Hu, Y., Shi, L., Guo, S., Li, Z. A Decoupling Three-Dimensional Motion Control Algorithm for Spherical Underwater Robot. Biomimetic Intelligence and Robotics, 2022, 2(3), 50-58. https://doi.org/10.1016/j.birob.2022.100067
2. Cetin, G., Kecebas, A. Optimization of Thermodynamic Performance with Simulated Annealing Algorithm: A Geothermal Power Plant. Renewable Energy, 2021, 968-982. https://doi.org/10.1016/j.renene.2021.03.101
3. Hao, X., Liu, J., Zhang, Y. Mathematical Model and Simulated Annealing Algorithm for Chinese High School Timetabling Problems Under the New Curriculum Innovation. Frontiers of Computer Science, 2021, 15(1), 167-177. https://doi.org/10.1007/s11704-020-9102-4
4. Jia, L., Chen, Y., Cheng, R., Tan, T., Song, K. Designing Method of Acceleration and Deceleration Control Schedule for Variable Cycle Engine. Chinese Journal of Aeronautics, 2020, 34(8), 27-38. https://doi.org/10.1016/j.cja.2020.08.037
5. Leng, X. K., Piao, S. H., Chang, L., He, Z. C., Zhu, Z., Zhou, S. Z. Parameter Design of Biped Robot Motion System Based on Multi-Objective Optimization. Journal of Intelligent & Fuzzy Systems, 2021, 41(3), 4307-4318. https://doi.org/10.3233/JIFS-189691
6. Li, S. J. Research Progress on Trajectory Planning of Industrial Robots. Current Journal of Applied Science and Technology, 2023, 42(2), 25-36. https://doi.org/10.9734/cjast/2023/v42i24052
7. Li, X., Yun, X., Zhao, Z., Zhang, K., Wang, X. Lightweight Deep Learning Method for Multi-Vehicle Object Recognition. Information Technology and Control, 2022, 51(2), 294-312. https://doi.org/10.5755/j01.itc.51.2.30667
8. Lin, J. Artificial Intelligence Control Algorithm for Steering Motion of Wheeled Soccer Robot. Journal of Intelligent & Fuzzy Systems: Applications in Engineering and Technology, 2020, 38(6), 7915-7923. https://doi.org/10.3233/JIFS-179860
9. Lin, J., Chiang, C. K. Motion Control of a Cable-Suspended Robot Using Image Recognition with Coordinate Transformation. Proceedings of the Institution of Mechanical Engineers Part I Journal of Systems and Control Engineering, 2020, 235(1), 52-67. https://doi.org/10.1177/0959651820932760
10. Liu, M., Lin, R., Yang, M., Nazarova, A. V., Huo, J. Active Disturbance Rejection Motion Control of Spherical Robot with Parameter Tuning. Industrial Robot, 2022, 49(2), 332-343. https://doi.org/10.1108/IR-05-2021-0099
11. Lu, Y., Shen, Y. C., Zhuang, C. G. External Force Estimation for Industrial Robots Using Configuration Optimization. Automatika, 2023, 64(2), 365-388. https://doi.org/10.1080/00051144.2023.2166451
12. Luo, H., Zhao, D., Fu, W. Speed Planning Algorithm Based on Improved S-Type Acceleration and Deceleration Model. Journal of Shanghai Jiaotong University (Science), 2021, 26(8), 786-793. https://doi.org/10.1007/s12204-021-2322-4
13. Qimin, X., Xin, Z., Longjie, L., Yameng, L., Na, L. Efficient and Accurate Vehicle Localization Based on LiDAR Place Recognition. Information Technology and Control, 2023, 52(2), 562-575. https://doi.org/10.5755/j01.itc.52.2.32690
14. Quenehen, A., Klement, N., Abdeljaouad, A. M., Roucoules, L., Gibaru, O. Economic and Ergonomic Performance Enhancement in Assembly Process Through Multiple Collaboration Modes Between Human and Robot. International Journal of Production Research, 2023, 61(5), 1517-1531. https://doi.org/10.1080/00207543.2022.2039795
15. Shao, J., Bian, Y. M., Yang, M., Liu, G. J. Characteristic Analysis and Motion Control of a Novel Ball Double-Screw Hydraulic Robot Joint. Engineering Applications of Computational Fluid Mechanics, 2022, 16(1), 1305-1323. https://doi.org/10.1080/19942060.2022.2080767
16. Shijin, Y., Huazhen, Z., Mi, L. I. CNOP-P-Based Parameter Sensitivity for Double-Gyre Variation in ROMS with Simulated Annealing Algorithm. Journal of Oceanology and Limnology, 2019, 37(3), 957-967. https://doi.org/10.1007/s00343-019-7266-2
17. Sundar, R., Kathirvel, A. Aggressively Delivered Mechanism Over Variable Length Density Using a Simulated Annealing Algorithm in Mobile Ad Hoc Network. Transactions on Emerging Telecommunications Tech-

nologies, 2020, 12(31), 1-13. https://doi.org/10.1002/ett.3863

18. Tufano, A., Accorsi, R., Manzini, R. A Simulated Annealing Algorithm for the Allocation of Production Resources in the Food Catering Industry. British Food Journal, 2020, 7(122), 2139-2158. https://doi.org/10.1108/BFJ-08-2019-0642
19. Wang, G., Wang, Q., Cui, X., Xu, S., Zhang, S. An Interpolation Algorithm of B-Spline Curve Based on S-Curve Acceleration/Deceleration with Interference Pre-Treatment. International Journal of Computer Applications in Technology, 2021, 66(1), 51-62. https://doi.org/10.1504/IJCAT.2021.119607
20. Xu, G. P., Meng, Z., Li, S., Sun, Y. Z. Collision-Free Trajectory Planning for Multi-Robot Simultaneous Motion in Preforms Weaving. Robotica, 2022, (40)12, 4218-4237. https://doi.org/10.1017/S026357472200087X
21. Yu, D. Y., Ding, Z., Tian, X. Q. Incomplete Smooth S-Curve Acceleration and Deceleration Feedrate Planning Modeling and Analysis. The International Journal of Advanced Manufacturing Technology, 2022, 120(11-12), 7171-7185. https://doi.org/10.1007/s00170-022-09236-7
22. Zadeh, N. H., Movahedi, M. M., Shayannia, S. A. Human Resource Scheduling in Project Management Using the Simulated Annealing Algorithm with the Human Factors Engineering Approach. Discrete Dynamics in Nature and Society, 2022, 1-7. https://doi.org/10.1155/2022/3597014
23. Zhao, J., Iwasaki, T. CPG Control for Harmonic Motion of Assistive Robot with Human Motor Control Identification. IEEE Transactions on Control Systems Technology, 2020, 28(4), 1323-1336. https://doi.org/10.1109/TCST.2019.2910160
24. Zhou, P., Yao, J. T., Zhang, H. Y., Zhang, X. H., Kong, S. Q., Zhu, K. M. Design and Kinematics of a Lightweight Cruciform Continuum Robot. Mechanical Sciences, 2023, 14(1), 99-109. https://doi.org/10.5194/ms-14-99-2023